

Generalization of a method by Mossotti for initial orbit determination

Giovanni F. Gronchi¹, Giulio Baù¹, Óscar Rodríguez¹, Robert Jedicke², and Joachim Moeyens³

¹Dipartimento di Matematica, Università di Pisa, Italy

²Institute for Astronomy, University of Hawai'i, USA

³Vera C. Rubin Observatory, University of Washington, USA

September 2, 2021

Abstract

Here we revisit an initial orbit determination method introduced by O. F. Mossotti employing four geocentric sky-plane observations and a linear equation to compute the angular momentum of the observed body. We then extend the method to topocentric observations, yielding a quadratic equation for the angular momentum. The performance of the two versions are compared through numerical tests with synthetic asteroid data using different time intervals between consecutive observations and different astrometric errors. We also show a comparison test with Gauss's method using simulated observations with the expected cadence of the VRO-LSST telescope.

1 Introduction

In 1816 Ottaviano F. Mossotti introduced a method for initial orbit determination of a solar system body employing four optical observations, e.g. the values of right ascension and declination. Assuming *geocentric* observations, Mossotti's method allows to write linear equations for the computation of the orbital angular momentum [17]. Then the orbit can be reconstructed, e.g. by Gibbs' method [10]. This procedure has the advantage to avoid the computation of the roots of the eight degree polynomial appearing in the classical methods by Laplace [13], Lagrange [12], and Gauss [5], which need only three observations but can give rise to multiple solutions. A review of the methods by Laplace and Gauss together with a geometric interpretation of the occurrence of multiple solutions can be found in [7], [14].

Mossotti's work was appreciated by Gauss himself, see [6]. This method has been reviewed in [1], where the authors state that the computation of the solution can be seriously affected by the observational errors due to the terms that are neglected in the employed approximation.

In this work we recall Mossotti's original method and show that it is possible to define a *topocentric* version which leads to a quadratic equation for the angular momentum. This generalization of the method turns out to be suitable for orbit determination of Earth satellites too. We investigate the performance of the methods and their sensitivity to observational

errors by some numerical tests with simulated data: we compare the original geocentric method with this topocentric version using different time intervals between the observations and different astrometric errors. We also show a comparison test with Gauss’s method using simulated observations with the expected cadence of the VRO-LSST telescope.

2 The original method

Mossotti’s method [17] leads to a set of linear equations for the components of $\mathbf{c}_\oplus - \mathbf{c}$, where \mathbf{c}_\oplus and \mathbf{c} are the angular momenta of the Earth and a solar system body, respectively. The observations are supposed to be made from the center of the Earth. We assume that the observed body is an asteroid, moving along an elliptic Keplerian trajectory with the Sun as the center of force. We also assume that the total observational arc is covered in a much shorter time than the orbital period. This method is also suitable to be used with hyperbolic or parabolic orbits.

Here we illustrate all the formulae which are necessary for a numerical implementation following Mossotti’s paper steps [17]. However, in the early XIXth century Linear Algebra had not been developed yet, and several formulae in [17] can be written and derived in a shorter way. The original formulae can be recovered using Table 3 in Appendix A.

2.1 Units and preliminary definitions

In order to simplify the notation we use the rescaled time θ , defined by

$$\theta = t \sqrt{g \left(1 + \frac{m_\oplus}{m_\odot} \right)},$$

where m_\oplus and m_\odot are the masses of the Earth and the Sun, and $g = Gm_\odot$, where G is Newton’s gravitational constant. We also use κ to denote Gauss’s constant \sqrt{g} . In the following we assume that

$$\theta \approx \kappa t,$$

neglecting the constant m_\oplus/m_\odot .

Take three of the four observations, at epochs $t_1 < t_2 < t_3$, and set

$$\begin{aligned} \theta_{ij} &= \kappa(t_j - t_i), \\ \boldsymbol{\theta} &= (\theta_{23}, \theta_{31}, \theta_{12})^t, \end{aligned}$$

where the superscript t stands for transposition. We write \mathbf{c} and \mathbf{c}_\oplus for the orbital angular momenta of the asteroid and the Earth, respectively, and introduce their unit vectors

$$\hat{\mathbf{c}} = \frac{\mathbf{c}}{c}, \quad \hat{\mathbf{c}}_\oplus = \frac{\mathbf{c}_\oplus}{c_\oplus},$$

where $c = |\mathbf{c}|$, $c_\oplus = |\mathbf{c}_\oplus|$, being $|\mathbf{x}|$ the Euclidean norm of a vector \mathbf{x} .

We also write \mathbf{r}_i and \mathbf{q}_i for the heliocentric positions of the asteroid and the Earth at the three epochs t_i ($i = 1, 2, 3$), use $\boldsymbol{\rho}_i = \mathbf{r}_i - \mathbf{q}_i$ for the geocentric position of the asteroid, and introduce the unit vectors

$$\hat{\mathbf{q}}_i = \frac{\mathbf{q}_i}{q_i}, \quad \hat{\boldsymbol{\rho}}_i = \frac{\boldsymbol{\rho}_i}{\rho_i}, \quad i = 1, 2, 3,$$

where $q_i = |\mathbf{q}_i|$, $\rho_i = |\boldsymbol{\rho}_i|$. Finally, we denote the parameters¹ of the orbits of the asteroid and the Earth by p , p_\oplus . They are defined by

$$p\kappa^2 = c^2, \quad p_\oplus\kappa^2 = c_\oplus^2.$$

2.2 Geometric relations

With the purpose of writing Mossotti's equations in a compact form, let us introduce the matrices

$$P = (\boldsymbol{\rho}_1 \mid \boldsymbol{\rho}_2 \mid \boldsymbol{\rho}_3), \quad Q = (\mathbf{q}_1 \mid \mathbf{q}_2 \mid \mathbf{q}_3), \quad R = P + Q = (\mathbf{r}_1 \mid \mathbf{r}_2 \mid \mathbf{r}_3), \quad (1)$$

where $(\mathbf{x}_1 \mid \mathbf{x}_2 \mid \mathbf{x}_3)$ is the matrix whose columns are the vectors \mathbf{x}_j . The corresponding adjugate matrices are

$$\begin{aligned} \text{adj}(P) &= (\boldsymbol{\rho}_2 \times \boldsymbol{\rho}_3 \mid \boldsymbol{\rho}_3 \times \boldsymbol{\rho}_1 \mid \boldsymbol{\rho}_1 \times \boldsymbol{\rho}_2)^t, \\ \text{adj}(Q) &= (\mathbf{q}_2 \times \mathbf{q}_3 \mid \mathbf{q}_3 \times \mathbf{q}_1 \mid \mathbf{q}_1 \times \mathbf{q}_2)^t, \\ \text{adj}(R) &= (\mathbf{r}_2 \times \mathbf{r}_3 \mid \mathbf{r}_3 \times \mathbf{r}_1 \mid \mathbf{r}_1 \times \mathbf{r}_2)^t. \end{aligned}$$

We recall the following property, which holds for any square matrix M :

$$M \text{adj}(M) = \text{adj}(M) M = \det(M) I, \quad (2)$$

where I is the identity matrix.

The rank of the matrices Q and R is 2, since each triplet $\{\mathbf{q}_1, \mathbf{q}_2, \mathbf{q}_3\}$ and $\{\mathbf{r}_1, \mathbf{r}_2, \mathbf{r}_3\}$ is made by coplanar vectors and we assume that

$$\mathbf{q}_i \times \mathbf{q}_j \neq \mathbf{0}, \quad \mathbf{r}_i \times \mathbf{r}_j \neq \mathbf{0}, \quad 1 \leq i < j \leq 3,$$

see Figure 1. This implies

$$Q \text{adj}(Q) = 0, \quad R \text{adj}(R) = 0. \quad (3)$$

Since the angular momenta \mathbf{c} , \mathbf{c}_\oplus are respectively orthogonal to the orbital planes of the asteroid and the Earth, we have

$$\mathbf{c} \cdot \mathbf{r}_i = \mathbf{c} \cdot (\mathbf{q}_i + \boldsymbol{\rho}_i) = 0, \quad \mathbf{c}_\oplus \cdot \mathbf{q}_i = 0,$$

which lead us to

$$\mathbf{c} \cdot \boldsymbol{\rho}_i = (\mathbf{c}_\oplus - \mathbf{c}) \cdot \mathbf{q}_i, \quad (4)$$

for $i = 1, 2, 3$. Then, we introduce the vectors

$$\boldsymbol{\tau} = (\tau_1, \tau_2, \tau_3)^t, \quad \mathbf{T} = (T_1, T_2, T_3)^t,$$

with

$$\tau_1 \sqrt{p} = \mathbf{r}_2 \times \mathbf{r}_3 \cdot \hat{\mathbf{c}}, \quad T_1 \sqrt{p_\oplus} = \mathbf{q}_2 \times \mathbf{q}_3 \cdot \hat{\mathbf{c}}_\oplus, \quad (5a)$$

$$\tau_2 \sqrt{p} = \mathbf{r}_3 \times \mathbf{r}_1 \cdot \hat{\mathbf{c}}, \quad T_2 \sqrt{p_\oplus} = \mathbf{q}_3 \times \mathbf{q}_1 \cdot \hat{\mathbf{c}}_\oplus, \quad (5b)$$

¹in [17] these are called *semiparametri*.

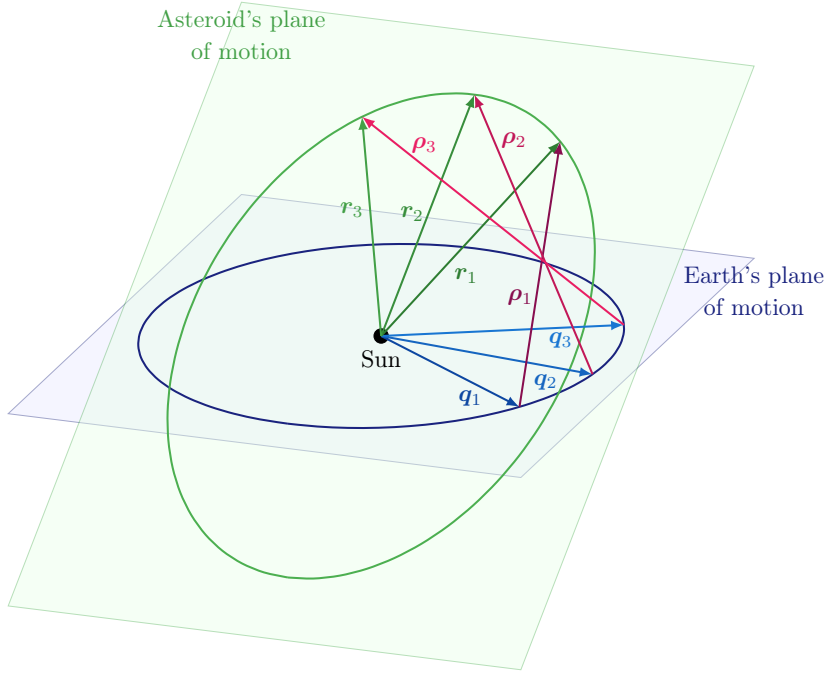


Figure 1: Geometry of the three observations.

$$\tau_3 \sqrt{p} = \mathbf{r}_1 \times \mathbf{r}_2 \cdot \hat{\mathbf{c}}, \quad T_3 \sqrt{p_\oplus} = \mathbf{q}_1 \times \mathbf{q}_2 \cdot \hat{\mathbf{c}}_\oplus. \quad (5c)$$

Noting that

$$\boldsymbol{\tau} = \frac{1}{\sqrt{p}} \text{adj}(R) \hat{\mathbf{c}}, \quad \mathbf{T} = \frac{1}{\sqrt{p_\oplus}} \text{adj}(Q) \hat{\mathbf{c}}_\oplus, \quad (6)$$

by (3) we have

$$R \boldsymbol{\tau} = \mathbf{0}, \quad Q \mathbf{T} = \mathbf{0}.$$

Moreover, recalling that $R = Q + P$, we get

$$P \boldsymbol{\tau} = Q(\mathbf{T} - \boldsymbol{\tau}). \quad (7)$$

Since $(\mathbf{r}_i \times \mathbf{r}_j) \times \mathbf{c} = (\mathbf{q}_i \times \mathbf{q}_j) \times \mathbf{c}_\oplus = \mathbf{0}$, we have

$$(\mathbf{r}_i \times \mathbf{r}_j \cdot \hat{\mathbf{c}})(\hat{\mathbf{c}} \cdot \boldsymbol{\rho}_i) = \mathbf{r}_i \times \mathbf{r}_j \cdot \boldsymbol{\rho}_i = \mathbf{q}_i \times \mathbf{q}_j \cdot \boldsymbol{\rho}_i - \boldsymbol{\rho}_i \times \boldsymbol{\rho}_j \cdot \mathbf{q}_i, \quad (8)$$

$$(\mathbf{q}_i \times \mathbf{q}_j \cdot \hat{\mathbf{c}}_\oplus)(\hat{\mathbf{c}}_\oplus \cdot \boldsymbol{\rho}_i) = \mathbf{q}_i \times \mathbf{q}_j \cdot \boldsymbol{\rho}_i. \quad (9)$$

Remark 1. *If the orbits of the Earth and the asteroid are almost coplanar, then the equations (8), (9) are close to be degenerate. This singularity is a common feature of orbit determination methods, where the value of the geodesic curvature of the observed arc plays an important role, see [14, Chap. 9].*

The last equality in (8) is obtained by observing that

$$\mathbf{r}_i \times \mathbf{r}_j \cdot \boldsymbol{\rho}_i = \mathbf{q}_i \times \mathbf{r}_j \cdot \boldsymbol{\rho}_i = \mathbf{q}_i \times \mathbf{q}_j \cdot \boldsymbol{\rho}_i + \mathbf{q}_i \times \boldsymbol{\rho}_j \cdot \boldsymbol{\rho}_i.$$

By (8), (9) and the definitions of the τ_k, T_k given in (5) we obtain

$$\varepsilon_{ijk} \frac{\tau_k}{\kappa} \mathbf{c} \cdot \boldsymbol{\rho}_i = \mathbf{q}_i \times \mathbf{q}_j \cdot \boldsymbol{\rho}_i - \boldsymbol{\rho}_i \times \boldsymbol{\rho}_j \cdot \mathbf{q}_i, \quad (10)$$

$$\varepsilon_{ijk} \frac{T_k}{\kappa} \mathbf{c}_\oplus \cdot \boldsymbol{\rho}_i = \mathbf{q}_i \times \mathbf{q}_j \cdot \boldsymbol{\rho}_i, \quad (11)$$

where ε_{ijk} denotes the Levi-Civita symbol, and the indexes i, j, k vary so that all the 6 permutations of the set $\{1, 2, 3\}$ can be considered.

Subtracting (10) from (11) we obtain

$$\varepsilon_{ijk} \frac{1}{\kappa} (T_k \mathbf{c}_\oplus - \tau_k \mathbf{c}) \cdot \boldsymbol{\rho}_i = \boldsymbol{\rho}_i \times \boldsymbol{\rho}_j \cdot \mathbf{q}_i. \quad (12)$$

Writing

$$T_k \mathbf{c}_\oplus - \tau_k \mathbf{c} = T_k (\mathbf{c}_\oplus - \mathbf{c}) + (T_k - \tau_k) \mathbf{c},$$

and using (4), we have

$$\begin{aligned} [T_k (\mathbf{c}_\oplus - \mathbf{c}) + (T_k - \tau_k) \mathbf{c}] \cdot \boldsymbol{\rho}_i &= T_k (\mathbf{c}_\oplus - \mathbf{c}) \cdot \boldsymbol{\rho}_i + (T_k - \tau_k) (\mathbf{c}_\oplus - \mathbf{c}) \cdot \mathbf{q}_i \\ &= (\mathbf{c}_\oplus - \mathbf{c}) \cdot \left[\hat{\boldsymbol{\rho}}_i + \left(1 - \frac{\tau_k}{T_k}\right) \frac{q_i}{\rho_i} \hat{\mathbf{q}}_i \right] T_k \rho_i. \end{aligned}$$

Therefore, introducing the coefficients

$$\alpha_{ik} = \left(1 - \frac{\tau_k}{T_k}\right) \frac{q_i}{\rho_i}, \quad (13)$$

and simplifying ρ_i we can write relations (12) as

$$\varepsilon_{ijk} (\mathbf{c}_\oplus - \mathbf{c}) \cdot (\hat{\boldsymbol{\rho}}_i + \alpha_{ik} \hat{\mathbf{q}}_i) T_k = \kappa \rho_j \hat{\boldsymbol{\rho}}_i \times \hat{\boldsymbol{\rho}}_j \cdot \mathbf{q}_i. \quad (14)$$

2.3 Combining geometry of observations with two-body dynamics

Since the time intervals θ_{12}, θ_{23} are small compared to the orbital period,² we can consider Taylor's expansions of the position of the asteroid and the center of the Earth in their orbital planes as power series of $\theta_{23}, \theta_{31}, \theta_{12}$ centering the expansion at the intermediate epoch. Then, we neglect the terms depending on the powers of θ_{ij} greater than 3. In this way we obtain

$$\boldsymbol{\tau} \simeq \boldsymbol{\theta} - \frac{1}{6r_2^3} \boldsymbol{\theta}^3, \quad \mathbf{T} \simeq \boldsymbol{\theta} - \frac{1}{6q_2^3} \boldsymbol{\theta}^3, \quad (15)$$

where $r_2 = |\mathbf{r}_2|$ and

$$\boldsymbol{\theta}^3 = \boldsymbol{\theta} \odot \boldsymbol{\theta} \odot \boldsymbol{\theta} = (\theta_{23}^3, \theta_{31}^3, \theta_{12}^3)^t,$$

with \odot denoting the Hadamard product.³

Let us define

$$\mathbf{u} = (u_1, u_2, u_3)^t = \text{adj}(\hat{P}) Q \boldsymbol{\theta}^3,$$

²the observations of asteroids at Mossotti's epoch were no more than one per night, and the time interval between two of them covered a few days.

³if $\mathbf{a} = (a_1, a_2, a_3)^t$ and $\mathbf{b} = (b_1, b_2, b_3)^t$, then $\mathbf{a} \odot \mathbf{b} = (a_1 b_1, a_2 b_2, a_3 b_3)^t$.

with $\hat{P} = (\hat{\rho}_1 | \hat{\rho}_2 | \hat{\rho}_3)$. Multiplying relation (7) on the left by $\text{adj}(\hat{P})$, and taking into account the approximations (15), we get

$$\begin{aligned} \text{adj}(\hat{P})P\boldsymbol{\theta} &\simeq \text{adj}(\hat{P})P\boldsymbol{\tau} = \text{adj}(\hat{P})Q(\mathbf{T} - \boldsymbol{\tau}) \\ &\simeq \text{adj}(\hat{P})Q\boldsymbol{\theta}^3 \left(\frac{1}{6r_2^3} - \frac{1}{6q_2^3} \right) = \frac{1}{6} \left(\frac{1}{r_2^3} - \frac{1}{q_2^3} \right) \mathbf{u}. \end{aligned} \quad (16)$$

Recalling (2), and noting that

$$\text{adj}(\hat{P})P = \det(\hat{P})\text{diag}\{\rho_1, \rho_2, \rho_3\},$$

relation (16) yields

$$\det(\hat{P})\boldsymbol{\delta} \odot \boldsymbol{\theta} \simeq \frac{1}{6} \left(\frac{1}{r_2^3} - \frac{1}{q_2^3} \right) \mathbf{u}, \quad (17)$$

with

$$\boldsymbol{\delta} = (\rho_1, \rho_2, \rho_3)^t.$$

2.4 A linear equation involving $\mathbf{c}_\oplus - \mathbf{c}$

Choosing $(i, j, k) = (1, 2, 3), (3, 2, 1)$ in (14) and eliminating $\kappa\rho_2$ from the two resulting equations, we obtain

$$\begin{aligned} (\hat{\rho}_1 \times \hat{\rho}_2 \cdot \mathbf{q}_1) [(\mathbf{c}_\oplus - \mathbf{c}) \cdot (\hat{\rho}_3 + \alpha_{31}\hat{\mathbf{q}}_3)] T_1 &= \\ (\hat{\rho}_2 \times \hat{\rho}_3 \cdot \mathbf{q}_3) [(\mathbf{c}_\oplus - \mathbf{c}) \cdot (\hat{\rho}_1 + \alpha_{13}\hat{\mathbf{q}}_1)] T_3. \end{aligned} \quad (18)$$

In this equation the only unknowns different from $(\mathbf{c}_\oplus - \mathbf{c})$ are the coefficients α_{13} and α_{31} . Using the approximations of $\boldsymbol{\tau}$ and \mathbf{T} given by (15) in (13) we have

$$\alpha_{13} = \frac{q_1 T_3 - \tau_3}{\rho_1 T_3} \simeq \frac{q_1}{\rho_1 T_3} \frac{\theta_{12}^3}{6} \left(\frac{1}{r_2^3} - \frac{1}{q_2^3} \right) \simeq \frac{q_1}{\rho_1} \frac{\theta_{12}^2}{6} \left(\frac{1}{r_2^3} - \frac{1}{q_2^3} \right), \quad (19)$$

where we used $\frac{1}{T_3} = \frac{1}{\theta_{12}}(1 + O(\theta_{12}))$. In a similar way we obtain

$$\alpha_{31} \simeq \frac{q_3}{\rho_3} \frac{\theta_{23}^2}{6} \left(\frac{1}{r_2^3} - \frac{1}{q_2^3} \right). \quad (20)$$

Inserting the approximations of ρ_1, ρ_3 given by (17) into (19), (20) we can express α_{13}, α_{31} with known quantities:

$$\alpha_{13} \simeq \frac{\det(\hat{P})q_1\theta_{12}^2\theta_{23}}{u_1}, \quad \alpha_{31} \simeq \frac{\det(\hat{P})q_3\theta_{23}^2\theta_{12}}{u_3}. \quad (21)$$

Defining the coefficients

$$a_1 = \frac{q_2 (\hat{\rho}_2 \times \hat{\rho}_3 \cdot \mathbf{q}_3)}{T_1 \sqrt{p_\oplus}} = \frac{\hat{\rho}_2 \times \hat{\rho}_3 \cdot \hat{\mathbf{q}}_3}{\hat{\mathbf{q}}_2 \times \hat{\mathbf{q}}_3 \cdot \hat{\mathbf{c}}_\oplus}, \quad a_3 = \frac{q_2 (\hat{\rho}_1 \times \hat{\rho}_2 \cdot \mathbf{q}_1)}{T_3 \sqrt{p_\oplus}} = \frac{\hat{\rho}_1 \times \hat{\rho}_2 \cdot \hat{\mathbf{q}}_1}{\hat{\mathbf{q}}_1 \times \hat{\mathbf{q}}_2 \cdot \hat{\mathbf{c}}_\oplus},$$

and the vectors

$$\boldsymbol{\gamma} = a_1 (\hat{\rho}_1 + \alpha_{13}\hat{\mathbf{q}}_1), \quad \boldsymbol{\varphi} = a_3 (\hat{\rho}_3 + \alpha_{31}\hat{\mathbf{q}}_3),$$

equation (18) becomes

$$(\boldsymbol{\gamma} - \boldsymbol{\varphi}) \cdot (\mathbf{c}_\oplus - \mathbf{c}) = 0. \quad (22)$$

Remark 2. Choosing the index pair $\{(2, 3, 1), (1, 3, 2)\}$ or $\{(3, 1, 2), (2, 1, 3)\}$ in (14) we can obtain two additional equations analogous to (22). However, with the employed approximation of \mathbf{T} and $\boldsymbol{\tau}$, the three equations are just the same (see [17, Sect. 28]).

2.5 Mossotti's equations for $\mathbf{c}_\oplus - \mathbf{c}$

With the aim of writing two independent linear equations, all the four observations are used. If we consider two different choices of the three observations, out of the available four, we obtain the system

$$\begin{cases} (\gamma_1 - \varphi_1) \cdot (\mathbf{c}_\oplus - \mathbf{c}) = 0 \\ (\gamma_2 - \varphi_2) \cdot (\mathbf{c}_\oplus - \mathbf{c}) = 0, \end{cases} \quad (23)$$

where the subscripts 1, 2 of γ and φ refer to the two triplets of observations. Set

$$\mathbf{w} = (\gamma_1 - \varphi_1) \times (\gamma_2 - \varphi_2)$$

and assume $\mathbf{w} \neq \mathbf{0}$. Then the general solution of (23) has the form

$$\mathbf{c}_\oplus - \mathbf{c} = \lambda \mathbf{w}, \quad (24)$$

with $\lambda \in \mathbb{R}$, giving the direction of $\mathbf{c}_\oplus - \mathbf{c}$.

Remark 3. *If $\gamma_1 - \varphi_1$ and $\gamma_2 - \varphi_2$ are almost parallel, then system (23) is almost degenerate: we can try to avoid this singularity by choosing other triplets of observations.*

In order to constrain the values of λ we proceed as follow. Choosing $(i, j, k) = (1, 2, 3)$ in equation (14), we have

$$\frac{a_3 c_\oplus \rho_2}{q_2} = (\mathbf{c}_\oplus - \mathbf{c}) \cdot (\hat{\boldsymbol{\rho}}_1 + \alpha_{13} \hat{\mathbf{q}}_1). \quad (25)$$

Inserting the expression (24) of the general solution in (25) and (4) with $i = 2$ we obtain, respectively,

$$\rho_2 = \lambda \frac{q_2}{a_1 a_3 c_\oplus} \mathbf{w} \cdot \boldsymbol{\gamma}_1, \quad (26)$$

and

$$\lambda \mathbf{w} \cdot \mathbf{q}_2 = (\mathbf{c}_\oplus - \lambda \mathbf{w}) \cdot \boldsymbol{\rho}_2 = (\mathbf{c}_\oplus - \lambda \mathbf{w}) \cdot \hat{\boldsymbol{\rho}}_2 \rho_2. \quad (27)$$

Substituting the expression (26) of ρ_2 in (27) yields a quadratic equation in λ , which is here the only unknown:

$$\lambda \mathbf{w} \cdot \mathbf{q}_2 = \lambda \frac{q_2}{a_1 a_3 c_\oplus} (\mathbf{w} \cdot \boldsymbol{\gamma}_1) [(\mathbf{c}_\oplus - \lambda \mathbf{w}) \cdot \hat{\boldsymbol{\rho}}_2].$$

This equation can be written as

$$(\mathbf{w} \cdot \boldsymbol{\gamma}_1)(\mathbf{w} \cdot \hat{\boldsymbol{\rho}}_2) \lambda^2 + [a_1 a_3 c_\oplus (\mathbf{w} \cdot \hat{\mathbf{q}}_2) - (\mathbf{w} \cdot \boldsymbol{\gamma}_1)(\mathbf{c}_\oplus \cdot \hat{\boldsymbol{\rho}}_2)] \lambda = 0, \quad (28)$$

whose solutions are

$$\lambda = 0, \quad (29a)$$

$$\lambda = \frac{(\mathbf{w} \cdot \boldsymbol{\gamma}_1)(\mathbf{c}_\oplus \cdot \hat{\boldsymbol{\rho}}_2) - a_1 a_3 c_\oplus (\mathbf{w} \cdot \hat{\mathbf{q}}_2)}{(\mathbf{w} \cdot \boldsymbol{\gamma}_1)(\mathbf{w} \cdot \hat{\boldsymbol{\rho}}_2)}. \quad (29b)$$

Substituting these expressions in (24) gives two possible values of the angular momentum \mathbf{c} . The solution (29a) yields $\mathbf{c}_\oplus = \mathbf{c}$, and is usually discarded, so that (29b) is regarded as the only solution. In this way the equations of Mossotti's method can be considered linear.

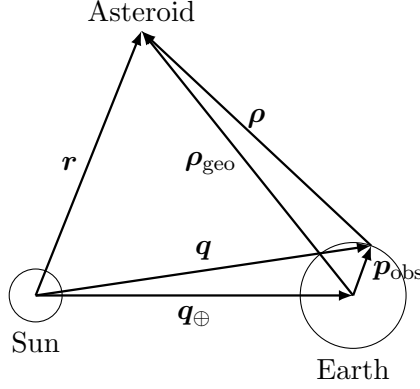


Figure 2: Geocentric and topocentric point of view.

3 Topocentric method

We first introduce some notation. Let us define \mathbf{q}_\oplus , \mathbf{p}_{obs} as the heliocentric position of the Earth center, and the geocentric position of the observer, respectively. The heliocentric positions of the observer and asteroid are

$$\begin{aligned}\mathbf{q} &= \mathbf{q}_\oplus + \mathbf{p}_{\text{obs}}, \\ \mathbf{r} &= \mathbf{q} + \boldsymbol{\rho} = \mathbf{q}_\oplus + \boldsymbol{\rho}_{\text{geo}},\end{aligned}$$

where $\boldsymbol{\rho}$, $\boldsymbol{\rho}_{\text{geo}}$ are the topocentric and geocentric positions of the asteroid, respectively (see Figure 2).

3.1 Geometric relations

As in the geocentric case, we select three observations of the asteroid out of the available four, and introduce the matrices P , Q , R as in (1), but with a different interpretation for the vectors $\boldsymbol{\rho}$ and \mathbf{q} : here $\boldsymbol{\rho}$ represents the topocentric position of the asteroid, and \mathbf{q} gives the heliocentric position of the observer. Moreover, we introduce the matrices

$$Q_\oplus = (\mathbf{q}_{\oplus,1} \mid \mathbf{q}_{\oplus,2} \mid \mathbf{q}_{\oplus,3}), \quad P_{\text{obs}} = (\mathbf{p}_{\text{obs},1} \mid \mathbf{p}_{\text{obs},2} \mid \mathbf{p}_{\text{obs},3}).$$

We recall the geometrical relations

$$\mathbf{c} \cdot \mathbf{r}_i = \mathbf{c} \cdot (\mathbf{q}_i + \boldsymbol{\rho}_i) = 0, \quad \mathbf{c}_\oplus \cdot \mathbf{q}_{\oplus,i} = \mathbf{c}_\oplus \cdot (\mathbf{q}_i - \mathbf{p}_{\text{obs},i}) = 0,$$

that lead us to

$$\mathbf{c} \cdot \boldsymbol{\rho}_i = (\mathbf{c}_\oplus - \mathbf{c}) \cdot \mathbf{q}_i - \mathbf{c}_\oplus \cdot \mathbf{p}_{\text{obs},i}, \quad (30)$$

for $i = 1, 2, 3$. We also introduce the quantities

$$\boldsymbol{\tau} = \frac{1}{\sqrt{p}} \text{adj}(R) \hat{\mathbf{c}}, \quad \mathbf{T} = \frac{1}{\sqrt{p_\oplus}} \text{adj}(Q_\oplus) \hat{\mathbf{c}}_\oplus, \quad (31)$$

which are the same as in (6), and define the matrix

$$\mathcal{C} = [\text{adj}(Q) - \text{adj}(Q_\oplus)] \hat{P}. \quad (32)$$

Like in the geocentric case, we have the relations

$$\varepsilon_{ijk} \frac{\tau_k}{\kappa} \mathbf{c} \cdot \boldsymbol{\rho}_i = \mathbf{q}_i \times \mathbf{q}_j \cdot \boldsymbol{\rho}_i - \boldsymbol{\rho}_i \times \boldsymbol{\rho}_j \cdot \mathbf{q}_i, \quad (33)$$

$$\varepsilon_{ijk} \frac{T_k}{\kappa} \mathbf{c}_\oplus \cdot \boldsymbol{\rho}_i + \mathcal{C}_{ki} \rho_i = \mathbf{q}_i \times \mathbf{q}_j \cdot \boldsymbol{\rho}_i, \quad (34)$$

where (i, j, k) is varied so that all the 6 permutations of the set $\{1, 2, 3\}$ are considered, and \mathcal{C}_{ki} denotes the element of the k -th row and i -th column of the matrix \mathcal{C} .

Subtracting (33) from (34) we obtain

$$\varepsilon_{ijk} \frac{1}{\kappa} (T_k \mathbf{c}_\oplus - \tau_k \mathbf{c}) \cdot \boldsymbol{\rho}_i + \mathcal{C}_{ki} \rho_i = \boldsymbol{\rho}_i \times \boldsymbol{\rho}_j \cdot \mathbf{q}_i, \quad (35)$$

and following the same procedure as in the geocentric case we can write (35) as

$$\varepsilon_{ijk} \left[(\mathbf{c}_\oplus - \mathbf{c}) \cdot (\hat{\boldsymbol{\rho}}_i + \alpha_{ik} \hat{\mathbf{q}}_i) + \frac{\kappa \mathcal{C}_{ki}}{T_k} - \frac{\alpha_{ik}}{q_i} \mathbf{c}_\oplus \cdot \mathbf{p}_{\text{obs},i} \right] T_k = \kappa \rho_j \hat{\boldsymbol{\rho}}_i \times \hat{\boldsymbol{\rho}}_j \cdot \mathbf{q}_i, \quad (36)$$

where the coefficients α_{ik} are defined as in (13), with the new interpretation for ρ_i and q_i .

Using the same approximations as in (15), we also note that

$$\begin{aligned} \text{adj}(\hat{P}) P \boldsymbol{\theta} &\simeq \text{adj}(\hat{P}) P \boldsymbol{\tau} = \text{adj}(\hat{P}) Q_\oplus (\mathbf{T} - \boldsymbol{\tau}) - \text{adj}(\hat{P}) P_{\text{obs}} \boldsymbol{\tau} \\ &\simeq \frac{1}{6} \left(\frac{1}{r_2^3} - \frac{1}{q_{\oplus,2}^3} \right) \mathbf{u} - \text{adj}(\hat{P}) P_{\text{obs}} \boldsymbol{\theta}, \end{aligned} \quad (37)$$

where $q_{\oplus,2} = |\mathbf{q}_{\oplus,2}|$ and

$$\mathbf{u} = (u_1, u_2, u_3)^t = \text{adj}(\hat{P}) Q_\oplus \boldsymbol{\theta}^3.$$

The presence of the term $\text{adj}(\hat{P}) P_{\text{obs}} \boldsymbol{\theta}$ in (37) prevents us from making the same simplification that allowed to express the α_{ik} as functions of known quantities. Noting that

$$\text{adj}(\hat{P}) P_{\text{obs}} = \mathcal{O}(p_{\text{obs}}),$$

where $p_{\text{obs}} = |\mathbf{p}_{\text{obs}}|$, we neglect this term and obtain

$$\det(\hat{P}) \boldsymbol{\delta} \odot \boldsymbol{\theta} \simeq \frac{1}{6} \left(\frac{1}{r_2^3} - \frac{1}{q_{\oplus,2}^3} \right) \mathbf{u},$$

with

$$\boldsymbol{\delta} = (\rho_1, \rho_2, \rho_3)^t.$$

As a consequence, the expressions for α_{13} and α_{31} given in (21) can still be used, with the new interpretation for the vectors $\boldsymbol{\rho}$ and \mathbf{q} .

3.2 A linear equation involving $\mathbf{c}_\oplus - \mathbf{c}$

Choosing $(i, j, k) = (1, 2, 3), (3, 2, 1)$ in (36) and eliminating $\kappa \rho_2$ from the resulting equations, we obtain

$$\begin{aligned} a_3 \left[(\mathbf{c}_\oplus - \mathbf{c}) \cdot (\hat{\boldsymbol{\rho}}_3 + \alpha_{31} \hat{\mathbf{q}}_3) + \frac{\kappa \mathcal{C}_{13}}{T_1} - \frac{\alpha_{31}}{q_3} \mathbf{c}_\oplus \cdot \mathbf{p}_{\text{obs},3} \right] = \\ a_1 \left[(\mathbf{c}_\oplus - \mathbf{c}) \cdot (\hat{\boldsymbol{\rho}}_1 + \alpha_{13} \hat{\mathbf{q}}_1) + \frac{\kappa \mathcal{C}_{31}}{T_3} - \frac{\alpha_{13}}{q_1} \mathbf{c}_\oplus \cdot \mathbf{p}_{\text{obs},1} \right], \end{aligned} \quad (38)$$

with

$$a_1 = \frac{(\hat{\boldsymbol{\rho}}_2 \times \hat{\boldsymbol{\rho}}_3 \cdot \mathbf{q}_3) q_2}{T_1 \sqrt{p_\oplus}} = \frac{(\hat{\boldsymbol{\rho}}_2 \times \hat{\boldsymbol{\rho}}_3 \cdot \mathbf{q}_3) q_2}{\mathbf{q}_{\oplus,2} \times \mathbf{q}_{\oplus,3} \cdot \hat{\mathbf{c}}_\oplus}, \quad a_3 = \frac{(\hat{\boldsymbol{\rho}}_1 \times \hat{\boldsymbol{\rho}}_2 \cdot \mathbf{q}_1) q_2}{T_3 \sqrt{p_\oplus}} = \frac{(\hat{\boldsymbol{\rho}}_1 \times \hat{\boldsymbol{\rho}}_2 \cdot \mathbf{q}_1) q_2}{\mathbf{q}_{\oplus,1} \times \mathbf{q}_{\oplus,2} \cdot \hat{\mathbf{c}}_\oplus}. \quad (39)$$

Like in the geocentric case, defining the vectors

$$\boldsymbol{\gamma} = a_1 (\hat{\boldsymbol{\rho}}_1 + \alpha_{13} \hat{\mathbf{q}}_1), \quad \boldsymbol{\varphi} = a_3 (\hat{\boldsymbol{\rho}}_3 + \alpha_{31} \hat{\mathbf{q}}_3),$$

we can write equation (38) as

$$(\boldsymbol{\gamma} - \boldsymbol{\varphi}) \cdot (\mathbf{c}_\oplus - \mathbf{c}) = D, \quad (40)$$

with

$$D = \kappa \left(\frac{a_3 \mathcal{C}_{13}}{T_1} - \frac{a_1 \mathcal{C}_{31}}{T_3} \right) + \left(\frac{a_1 \alpha_{13}}{q_1} \mathbf{p}_{\text{obs},1} - \frac{a_3 \alpha_{31}}{q_3} \mathbf{p}_{\text{obs},3} \right) \cdot \mathbf{c}_\oplus.$$

Remark 4. We can add to (40) two equations choosing the index pairs $\{(2, 3, 1), (1, 3, 2)\}$ and $\{(3, 1, 2), (2, 1, 3)\}$ in (36). In this way, we can write a linear system of three equations for $\mathbf{c}_\oplus - \mathbf{c}$ using only three observations. However, we expect that the matrix of this system is ill-conditioned because $Q = Q_\oplus + \mathcal{O}(p_{\text{obs}})$, so that the vectors $\mathbf{q}_1, \mathbf{q}_2, \mathbf{q}_3$ are almost coplanar.

3.3 Equations of the topocentric method

Following Section 2.5, if we consider two different choices of the three observations, we obtain the system

$$\begin{cases} (\boldsymbol{\gamma}_1 - \boldsymbol{\varphi}_1) \cdot (\mathbf{c}_\oplus - \mathbf{c}) = D_1 \\ (\boldsymbol{\gamma}_2 - \boldsymbol{\varphi}_2) \cdot (\mathbf{c}_\oplus - \mathbf{c}) = D_2. \end{cases} \quad (41)$$

Set

$$\mathbf{w} = (\boldsymbol{\gamma}_1 - \boldsymbol{\varphi}_1) \times (\boldsymbol{\gamma}_2 - \boldsymbol{\varphi}_2),$$

and assume $\mathbf{w} \neq \mathbf{0}$. Then the general solution of (41) takes the form

$$\mathbf{c}_\oplus - \mathbf{c} = \lambda \mathbf{w} + \mathbf{g}, \quad (42)$$

where $\lambda \in \mathbb{R}$, and \mathbf{g} is a particular solution of (41), e.g. the one fulfilling $\mathbf{g} \cdot \mathbf{w} = 0$.

In order to constrain the values of λ we proceed as follow. Note that we can write (36) with $(i, j, k) = (1, 2, 3)$ as

$$\frac{a_3 c_\oplus \rho_2}{q_2} = (\mathbf{c}_\oplus - \mathbf{c}) \cdot (\hat{\boldsymbol{\rho}}_1 + \alpha_{13} \hat{\mathbf{q}}_1) + \frac{\kappa \mathcal{C}_{31}}{T_3} - \frac{\alpha_{13}}{q_1} \mathbf{c}_\oplus \cdot \mathbf{p}_{\text{obs},1}. \quad (43)$$

Inserting the general solution (42) into (43) and (30) with $i = 2$ we obtain

$$\rho_2 = \frac{1}{b} (\lambda \mathbf{w} + \mathbf{g}) \cdot \boldsymbol{\gamma}_1 + f, \quad (44)$$

where

$$b = \frac{a_1 a_3 c_\oplus}{q_2}, \quad f = \frac{q_2}{a_3 c_\oplus} \left(\frac{\kappa \mathcal{C}_{31}}{T_3} - \frac{\alpha_{13}}{q_1} \mathbf{c}_\oplus \cdot \mathbf{p}_{\text{obs},1} \right), \quad (45)$$

and

$$(\mathbf{c}_\oplus - \lambda \mathbf{w} - \mathbf{g}) \cdot \hat{\boldsymbol{\rho}}_2 \rho_2 = (\lambda \mathbf{w} + \mathbf{g}) \cdot \mathbf{q}_2 - \mathbf{c}_\oplus \cdot \mathbf{p}_{\text{obs},2}. \quad (46)$$

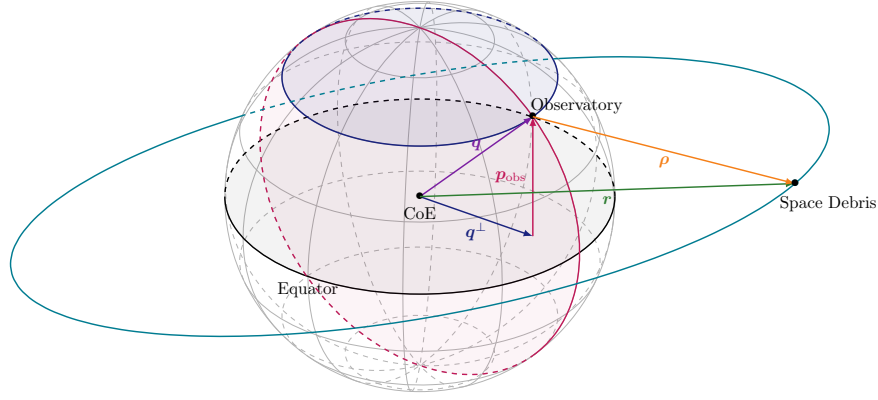


Figure 3: Geometry of observations of space debris.

Substituting the expression (44) of ρ_2 in (46) we get

$$(\mathbf{c}_\oplus - \lambda \mathbf{w} - \mathbf{g}) \cdot \hat{\rho}_2 \left[\frac{1}{b} (\lambda \mathbf{w} + \mathbf{g}) \cdot \gamma_1 + f \right] = (\lambda \mathbf{w} + \mathbf{g}) \cdot \mathbf{q}_2 - \mathbf{c}_\oplus \cdot \mathbf{p}_{\text{obs},2},$$

which can be written as

$$\begin{aligned} & (\mathbf{w} \cdot \gamma_1)(\mathbf{w} \cdot \hat{\rho}_2)\lambda^2 + [(\mathbf{w} \cdot \mathbf{q}_2)b - (\mathbf{w} \cdot \gamma_1)(\mathbf{c}_\oplus - \mathbf{g}) \cdot \hat{\rho}_2 + (\mathbf{w} \cdot \hat{\rho}_2)(\mathbf{g} \cdot \gamma_1 + bf)]\lambda \\ & + b(\mathbf{g} \cdot \mathbf{q}_2 - \mathbf{c}_\oplus \cdot \mathbf{p}_{\text{obs},2}) - (\mathbf{g} \cdot \gamma_1 + bf)(\mathbf{c}_\oplus - \mathbf{g}) \cdot \hat{\rho}_2 = 0. \end{aligned} \quad (47)$$

Equation (47) can be compared with equation (28). It is worth noting that in the topocentric formulation we do not have the solution $\lambda = 0$ as in Mossotti's original method, so that this formulation leads to a quadratic equation.

Remark 5. *In the topocentric case we could add a third linear equation to system (41) by choosing three different triplets of observations, out of the available four. However, we expect that also in this case the system is ill-conditioned, because the vectors $\mathbf{q}_1, \mathbf{q}_2, \mathbf{q}_3, \mathbf{q}_4$ are almost coplanar.*

4 Mossotti's method for space debris

We can follow the same scheme introduced in Section 3 for the computation of the orbits of space debris, assuming that the Earth is spherical and rotates with uniform angular velocity. In this case we use the rescaled time

$$\theta = \kappa_\oplus t,$$

with $\kappa_\oplus = \sqrt{Gm_\oplus}$. Here the vector \mathbf{q} represents the geocentric positions of the observer, \mathbf{r} and $\boldsymbol{\rho} = \mathbf{r} - \mathbf{q}$ give the geocentric and topocentric positions of the debris, and $\mathbf{c} = \mathbf{r} \times \dot{\mathbf{r}}$ is its orbital angular momentum. We consider the orthogonal decomposition

$$\mathbf{q} = \mathbf{q}^\perp + \mathbf{p}_{\text{obs}},$$

with

$$\mathbf{q}^\perp = (\mathbf{e}_3 \times \mathbf{q}) \times \mathbf{e}_3, \quad \mathbf{p}_{\text{obs}} = (\mathbf{q} \cdot \mathbf{e}_3)\mathbf{e}_3,$$

where \mathbf{e}_3 is the unit vector of the Earth rotation axis, see Figure 3. Moreover, we introduce the vector

$$\mathbf{c}_{\text{obs}} = \mathbf{q}^\perp \times \frac{d}{dt}\mathbf{q}^\perp = \mathbf{q}^\perp \times \dot{\mathbf{q}},$$

where the last equality holds because \mathbf{p}_{obs} is constant.

We can write a quadratic equation analogous to (47) simply by substituting the vectors \mathbf{c}_\oplus , \mathbf{q}_\oplus with \mathbf{c}_{obs} , \mathbf{q}^\perp , and the parameter p_\oplus with $|\mathbf{q}^\perp|$.

5 Numerical tests

In this section we test the performance of Mossotti’s original geocentric method (see Section 2) and its topocentric version introduced in Section 3. In the following, we denote the former by M_{geo} and the latter by M_{top} .

In Sections 5.1, 5.2 we compare M_{geo} with M_{top} using simulated observations (right ascension and declination) computed for the site of the Pan-STARRS1 telescope, mount Haleakala, Hawaii, without taking into account observability conditions, i.e. the asteroids are not necessarily visible in the night sky. Moreover, we assume that the four observations given in input to M_{geo} and M_{top} are equally spaced in time. The time interval Δt between two consecutive observations is varied in the two intervals:

$$I_1 = [15, 200] \text{ minutes}, \quad I_2 = [0.25, 100] \text{ days}. \quad (48)$$

The comparison is based on the computation of the angular momentum vector \mathbf{c} and the following related quantities: its magnitude $c = |\mathbf{c}|$ and direction $\hat{\mathbf{c}} = \mathbf{c}/c$, the longitude of the (ascending) node Ω , and the inclination i . We denote by x_t the *true* value of the quantity x , and by x_{geo} , x_{top} the values of x computed by M_{geo} , M_{top} , respectively. Note that while M_{geo} always produces one solution for \mathbf{c} , the method M_{top} can give two solutions. If this is the case, we select the one for which $|\mathbf{c}_t - \mathbf{c}_{\text{top}}|$ is smaller.

In Section 5.3 the method M_{top} is compared to Gauss’s method for initial orbit determination. Synthetic data have been obtained that take into account the observability conditions and the expected real cadence of the observations from the Vera C. Rubin Observatory, which is currently under construction in Chile. With respect to the previous tests, we remark that for any set of four observations the time interval Δt is not constant.

5.1 Tests without astrometric errors

We consider simulated observations of the asteroid Vesta without astrometric error. The time Δt between two consecutive observations is varied in the two intervals I_1 , I_2 specified in (48). Given Δt , we select 10^5 different initial epochs in a random way, and for each of them we generate four observations. For this purpose, we use the orbit of Vesta at the epoch 59200 MJD from the AstDysS-2 website⁴ and propagate it to the desired epochs assuming Keplerian motion. The angular momentum vector defined by the Keplerian orbit is assumed to be the true solution (\mathbf{c}_t). Finally, we apply M_{geo} , M_{top} to each set of four observations.

⁴<https://newton.spacedys.com/astdys/>, last access February 13, 2021.

Let us first consider the case of short arcs of observation. For each Δt selected in I_1 we compute the differences between the true values of the inclination (i_t), longitude of the node (Ω_t), magnitude of the angular momentum vector (c_t) of Vesta, and the values obtained by either M_{geo} or M_{top} . Some relevant statistical quantities related to these errors are shown in Figure 4 as functions of Δt . We note that the topocentric version of Mossotti’s method provides much better results than the original method. In particular, we observe that the performance of M_{top} improves as Δt increases, and it stabilizes when the time interval is about 30 minutes. It is remarkable that for Δt larger than 25 minutes the error in the inclination is smaller than 0.01 degrees for the solutions that fall within the 1st and 3rd quartile and it is smaller than 0.1 degrees for the solutions that fall within the 5th and 95th percentile.

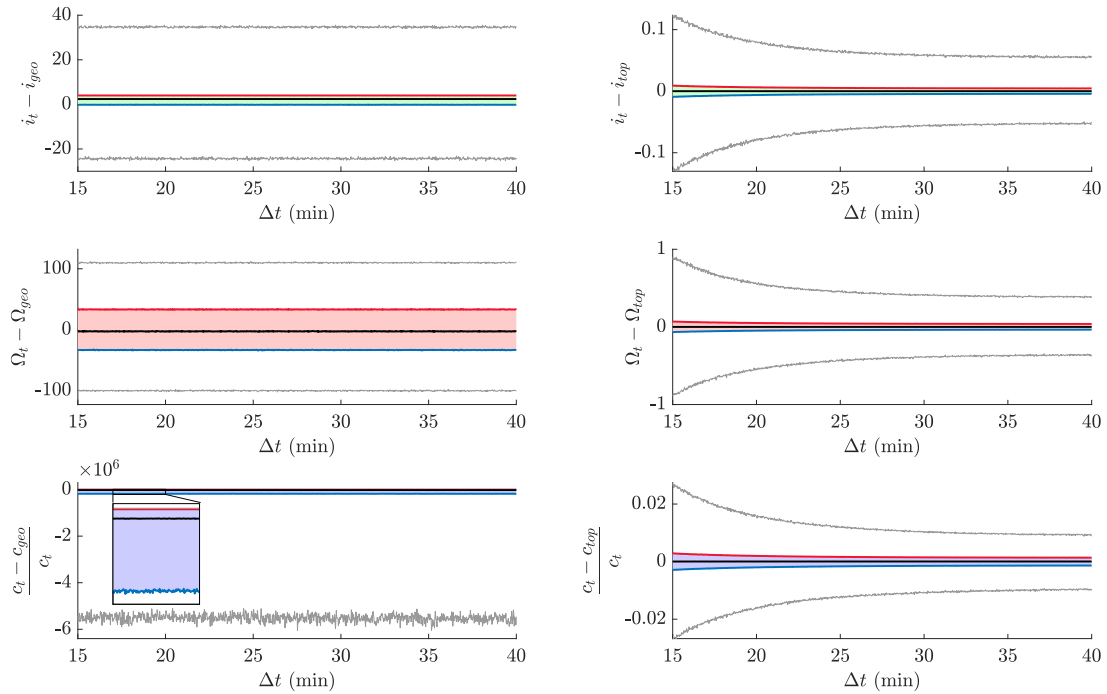


Figure 4: Statistics related to the errors in the inclination i , longitude of the node Ω , and magnitude of the angular momentum vector c , obtained by M_{geo} (left) and M_{top} (right) as functions of Δt in the case of observations of Vesta without astrometric error. In particular, we show the median (black line), the 1st and 3rd quartiles (blue and red lines), and the 5th and 95th percentiles (gray lines). The angles are in degrees and the Δt step is 1.5 seconds.

We then allow Δt to take values in the interval I_2 , which corresponds to wider arcs of observation. For each Δt selected in I_2 we compute the errors in the angular momentum vector and its direction. Statistical quantities related to these errors are shown in Figure 5 as functions of Δt . M_{top} continues to show better results and a smoother behavior for values of Δt smaller than 30 days, even if the improvement over M_{geo} is less pronounced with respect to that shown in Figure 4. In such interval, the geocentric method is much more sensitive to Δt and large oscillations having a period of one day appear. This is due to not accounting for the topocentric position of the observer. We also notice that both methods exhibit an

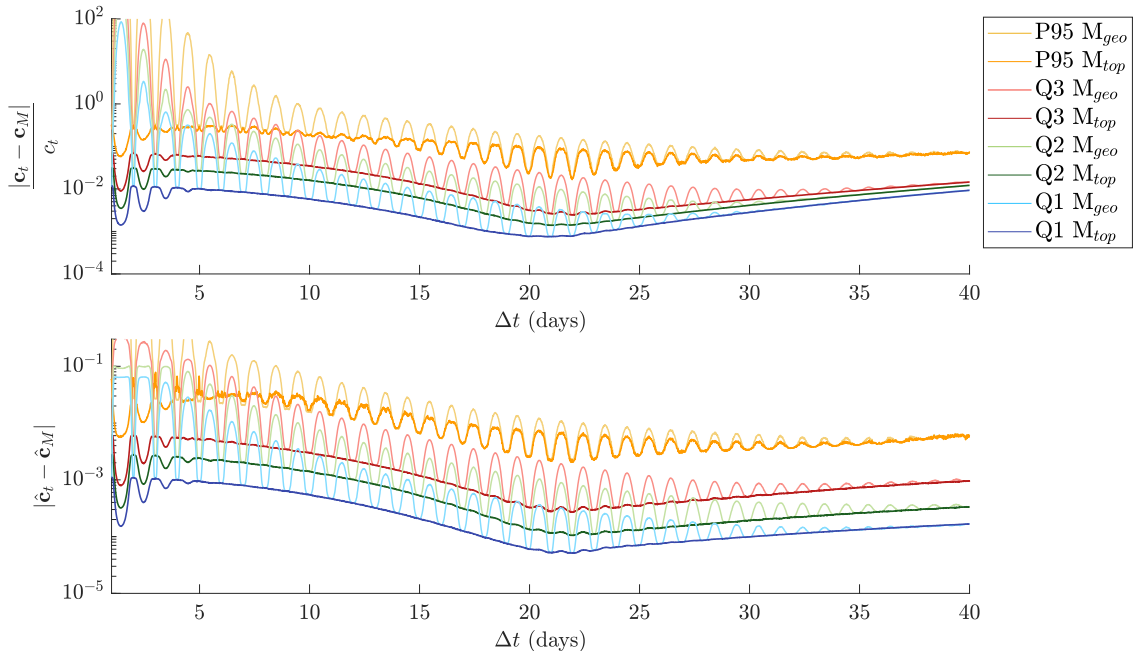


Figure 5: Statistics related to the errors in the angular momentum vector \mathbf{c} and its direction $\hat{\mathbf{c}}$, obtained by M_{geo} and M_{top} as functions of Δt in the case of observations of Vesta without astrometric error. In particular, we show the median (Q2), the 1st and 3rd quartiles (Q1, Q3), and the 95th percentile (P95). Here the Δt step is 15 minutes.

optimal performance for $\Delta t \approx 3$ weeks, and M_{top} obtains in 75% of the solutions an error smaller than 0.2% and 0.03% in the vectors \mathbf{c} and $\hat{\mathbf{c}}$, respectively.

If we consider time intervals longer than 30 days, the performance of the two methods is almost comparable, which is expected because the terms introduced in the topocentric version become smaller as Δt grows. The solutions with both methods deteriorate for $\Delta t > 80$ days since they rely on Taylor’s expansions with respect to Δt .

In Table 1 we report the inclination, longitude of the node, and magnitude of the angular momentum vector obtained by M_{geo} and M_{top} from observations of Vesta without astrometric error, considering different values of Δt with the same epoch for the first observation. We also show for M_{geo} with the label “2” the solution of Mossotti’s original method which is always discarded, i.e. the one for which the angular momenta of the asteroid and the Earth are equal. We observe that if Δt is large enough, the values of i and c of this spurious solution are close to the *wrong* solution from M_{top} (also labeled by “2”). The same behavior is not observed for Ω because the Earth orbital inclination is small and therefore small variations in i can cause large deviations in Ω . For $\Delta t = 30$ minutes (0.02 days) the solution from M_{geo} with label “1” is very close to the wrong solution from M_{top} : in this case only M_{top} gives values of i , Ω , c close to the true ones.

5.2 Tests with astrometric errors

The same numerical tests described in the previous section for the asteroid Vesta are carried out by introducing an astrometric error with zero mean and standard deviation (rms) of 0.1

Δt (days)	0.02	1	10	50	100	True value
i_1 (geo)	17.80160	7.06410	7.20588	7.09387	7.05670	7.14165
i_2 (geo)	0.00315	0.00297	0.00303	0.00436	0.00278	
i_1 (top)	7.14611	7.06413	7.20572	7.09407	7.05700	
i_2 (top)	17.79875	0.00156	0.00328	0.00305	0.00881	
Ω_1 (geo)	150.28159	103.18144	104.36892	103.20691	105.07597	103.80838
Ω_2 (geo)	140.61411	146.13681	-143.70328	160.84846	179.83017	
Ω_1 (top)	103.83824	103.17391	104.35977	103.19931	105.07223	
Ω_2 (top)	150.27855	167.05122	-112.30086	-174.23000	-66.15466	
c_1 (geo)	1125.88148	0.02600	0.02650	0.02694	0.03463	0.02633
c_2 (geo)	0.01721	0.01721	0.01719	0.01720	0.01719	
c_1 (top)	0.02628	0.02600	0.02650	0.02694	0.03463	
c_2 (top)	1124.55534	0.01720	0.01719	0.01720	0.01718	

Table 1: Values of the inclination (i), longitude of the node (Ω), magnitude of the angular momentum vector (c), obtained by M_{top} and M_{geo} , with observations of Vesta not affected by astrometric error and with different time intervals between consecutive observations. The epoch of the true orbit is 59200 MJD, the epoch of the first observation is ~ 59200.012 MJD (due to aberration correction), and the angles are in degrees.

arcsec in the values of right ascension and declination, which is typical of modern asteroid surveys like Pan-STARRS1. Neither M_{geo} nor M_{top} gives reliable results for Δt between 15 and 200 minutes. Indeed, determining a preliminary orbit from a single short arc is a challenging task, sometimes impossible without considering infinitely many solutions [16], [15]. However, the computation of a preliminary orbit can be performed by linking together two or more short arcs (e.g. [8], [9]). On the other hand, both methods yield satisfactory results for time intervals between two consecutive observations larger than 8 hours with only a slight degradation of their performance with the introduction of astrometric error (compare Figures 5 and 6). As in the case without astrometric error, M_{top} is better than M_{geo} for any considered Δt . A smoother behavior of M_{top} is observed for Δt smaller than 30 days. Both methods perform best for $\Delta t \approx 3$ weeks.

In our third test we use M_{geo} and M_{top} with synthetic observations of the 546077 numbered asteroids known to the date of October 19, 2020. Their orbital elements at the epoch 59200 MJD (from AstDyS-2) provide the true orbit and are used to simulate observations from the Pan-STARRS1 telescope site. The epoch of the first observation is obtained from 59200 MJD considering aberration correction; then the subsequent three observations are simulated by Keplerian propagation. The time Δt is varied in the interval I_2 given in (48), and the standard deviation of the astrometric error spans from 0 to 1 arcsec. Figures 7, 8 show that for time intervals between 20 and 40 days both M_{geo} and M_{top} give good results. A closer look at this range of values of Δt for M_{geo} reveal the same oscillations displayed in Figures 5 and 6. On

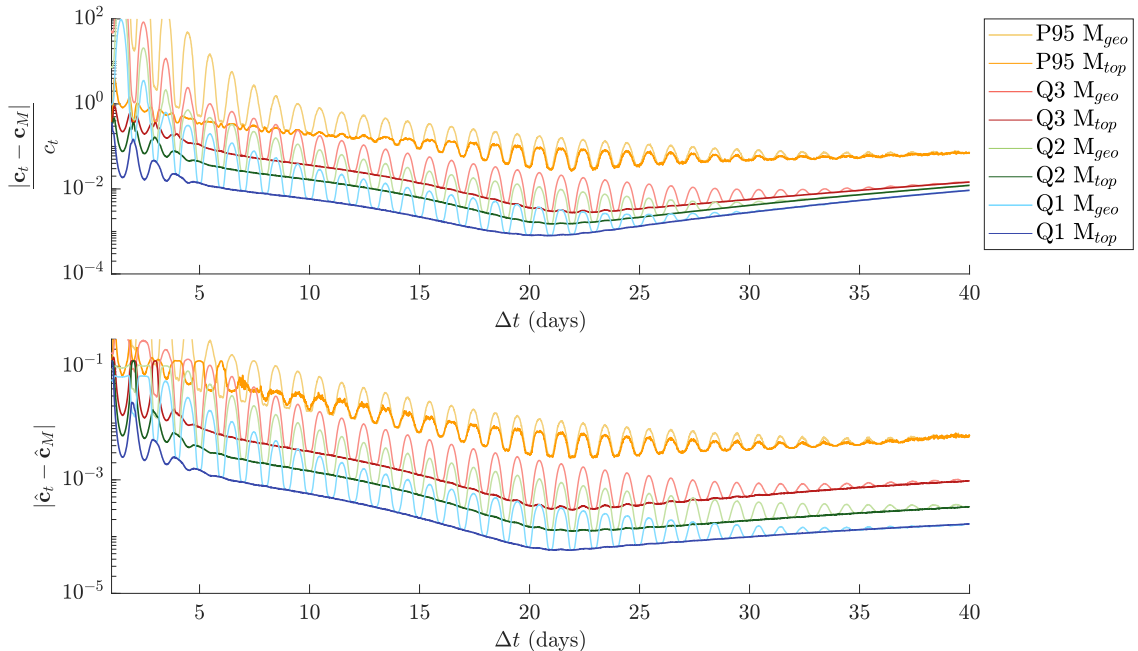


Figure 6: Same as Figure 5 but the observations of Vesta are affected by astrometric error with zero mean and rms of 0.1 arcsec. Here the Δt step is 15 minutes.

the other hand, M_{top} smooths out such oscillations. The best performance of both M_{geo} and M_{top} is reached again for $\Delta t \approx 3$ weeks.

5.3 Tests on synthetic survey data without astrometric errors

Our final test introduces more realism into the simulations in an attempt to assess the performance of the topocentric version of Mossotti’s method (M_{top}) on synthetic data that uses a realistic cadence and accounts for actual observability of the asteroids. With the motivation that Mossotti’s initial orbit determination method could be applied to linking observations of unknown asteroids in contemporary and future asteroid surveys, we applied M_{top} to synthetic observations from the Vera Rubin Observatory’s (VRO) Legacy Survey of Space and Time (LSST) [11]. They have developed a high-fidelity survey scheduler that will be employed in final operations but is currently being used to simulate and optimize the survey strategy [2, 3, 18]. We used a single survey simulation for one month of surveying that did not include any astrometric error. Then we extracted the first four synthetic detections of all the detected numbered NEOs, Trojans, Centaurs, and TNOs, but only a small subset of the detected main belt objects so that they would not dominate our results. The epochs of observation were all within about 30 days and the astrometric positions were generated with a full n -body integration. This process produced a set of four detections of 1535 objects distributed throughout the solar system. We then processed all the detections with both M_{top} and our implementation of Gauss’s method, by limiting our search to bounded orbits only.

In our sample Gauss’s method was able to produce orbits for 1493 objects (i.e. $\sim 97\%$) and M_{top} provided solutions for 1395 objects (i.e. $\sim 91\%$). However, we had 59 occurrences of a negative discriminant of equation (47) with M_{top} , and for some of them we were able to

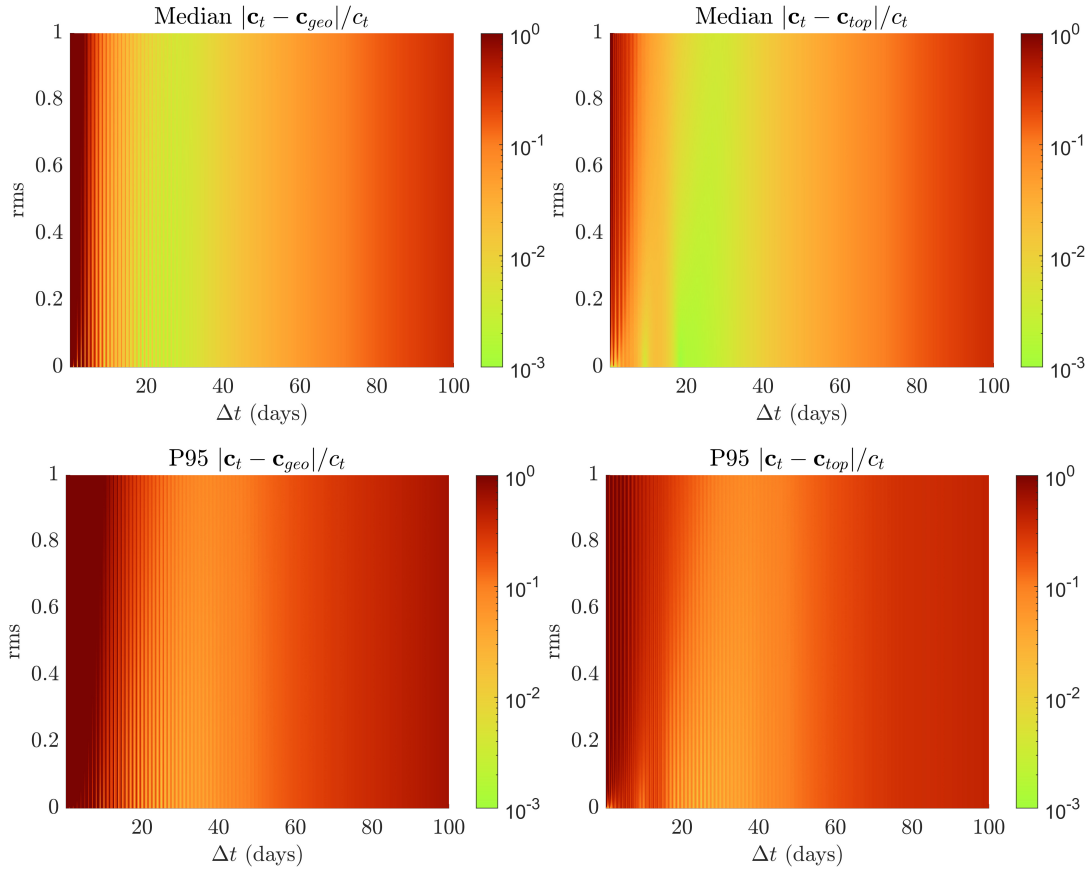


Figure 7: Performance of Mossotti’s original method (*left*) and its topocentric version (*right*) with observations of 546077 numbered asteroids. For each asteroid we compute the difference between the true angular momentum vector \mathbf{c}_t at the epoch 59200 MJD, and the same quantity \mathbf{c} obtained by either M_{geo} or M_{top} on a uniform grid of values of Δt and rms of the astrometric error in the intervals $[0.25, 100]$ days and $[0, 1]$ arcsec. Colored representations of the median and the 95th percentile related to the error $|\mathbf{c}_t - \mathbf{c}|/c_t$ are displayed. The step of Δt is 6 hours, the step of rms is 0.002 arcsec.

recover an acceptable orbit by setting the discriminant equal to zero. Doing so increases the number of solutions for M_{top} to 1454 (i.e. $\sim 95\%$).

While Gauss’s method can yield three different solutions for the same set of observations and M_{top} can yield two, on this set of data they had multiple solutions for about 50% and 45% of the objects, respectively. Gauss’s method did not produce any orbit for 42 objects and M_{top} for 81. Moreover, both of them failed in 30 of these cases. In 12 cases M_{top} was able to obtain at least one orbit while Gauss’s method was not, and for some cases it found an acceptable orbit.

The primary benefit of M_{top} is that in our limited testing it appears to be about 6 times faster than Gauss’s method. We repeated the orbit computation 1000 times for each of the 1535 objects using an Intel Xeon processor, with base clock 3.30 GHz: Gauss’s algorithm took ~ 77 seconds, while $M_{top} \sim 13$ seconds.

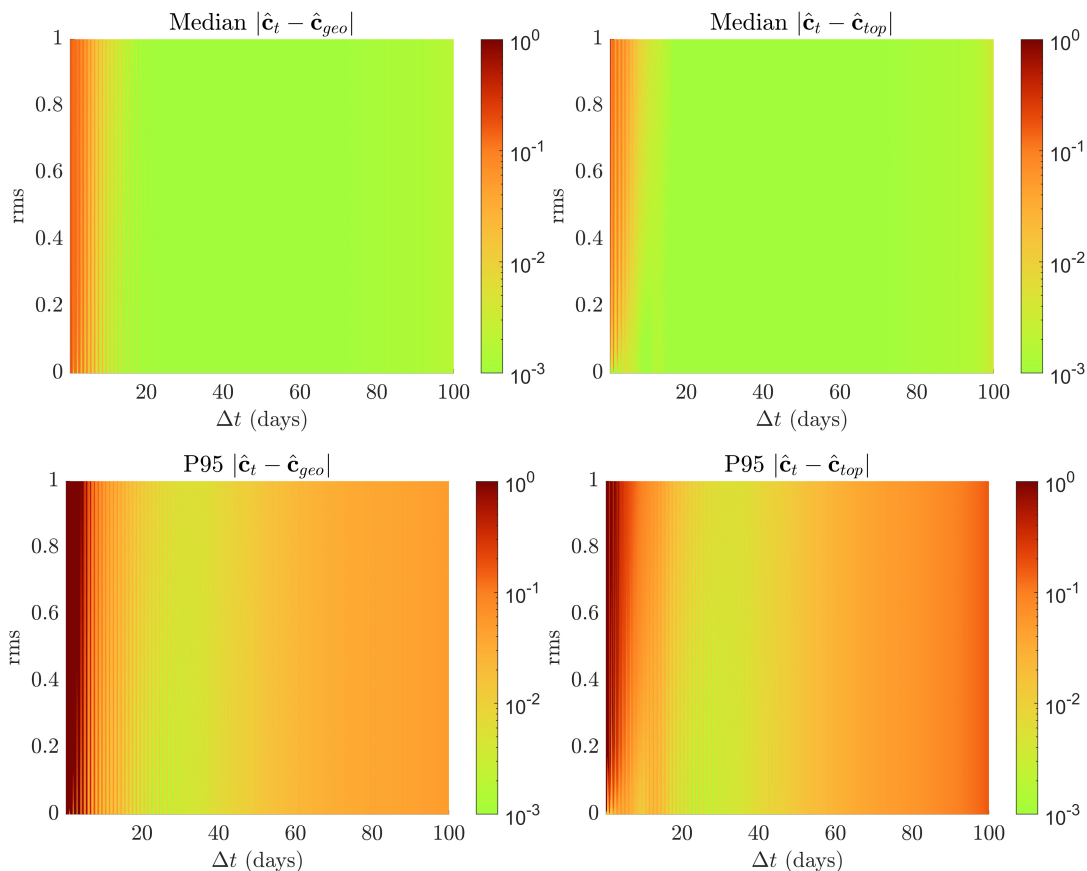


Figure 8: Same as Figure 7 for the error in the direction of the angular momentum vector.

Gauss’s technique provides better solutions for objects throughout the solar system (Figure 9 and Table 2). When comparing the derived orbital elements with their actual values we used the derived orbit solution that had the lowest 5-element D -criterion⁵ relative to the actual orbit [4]. A simple visual comparison of the results suggests that Gauss’s method is more likely to produce good orbital elements and less likely to yield wildly different values. Quantitative orbital element comparisons confirm this impression (Table 2).

6 Conclusions

In this paper we have revisited Mossotti’s orbit determination method working with four geocentric observations of a celestial body, and extended it to the case of topocentric observations. While Mossotti’s method yields linear equations for the components of the angular momentum vector, the topocentric version leads to a quadratic equation. Numerical simulations with synthetic observations both without and with astrometric error show that the topocentric method improves the original one. Considering all the numbered asteroids, and generating for each of them four observations equally spaced in time, we find that both these

⁵The D -criterion quantifies the difference between two orbits using all the orbital elements except for the mean anomaly.

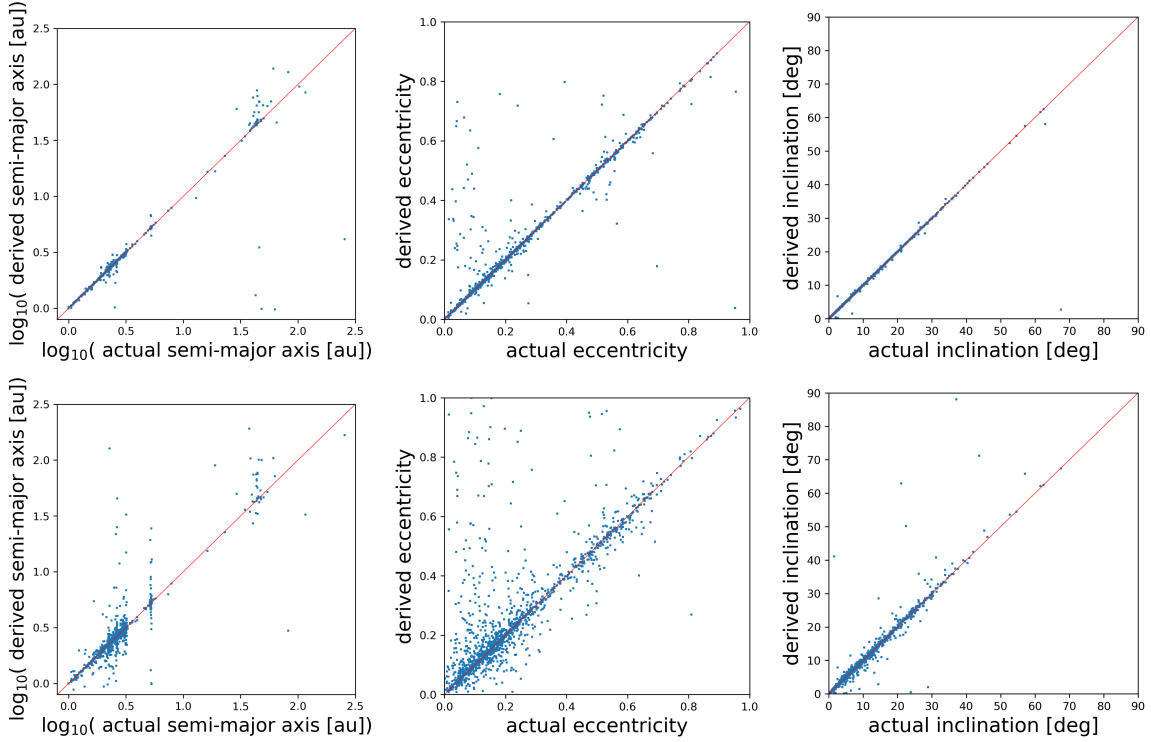


Figure 9: All the panels present the derived orbital parameter on the y -axis versus the actual parameter value on the x -axis using error-free data from a VRO-LSST simulation. The top panels are for Gauss’s method and the bottom panels use the topocentric version of Mossotti’s method. From left to right the panels compare $\log_{10}(a/[au])$, where a is the semi-major axis, eccentricity, and inclination. The red reference line in each figure has a slope of 1.

orbital element	Gauss		Mossotti	
	$\bar{\Delta}$	rms	$\bar{\Delta}$	rms
semi-major axis (au)	0.13	3.44	0.28	3.18
eccentricity	0.01	0.07	0.03	0.12
inclination (deg)	-0.02	0.27	0.05	2.31
long. node (deg)	-0.09	1.83	0.10	4.58
arg. perihelion (deg)	-0.38	8.51	0.10	19.17

Table 2: Mean and rms of the difference between the actual and derived orbital elements for both Gauss’s method and the topocentric version of Mossotti’s method. For the angular elements we eliminated some outliers to better illustrate the difference between the methods in the vast majority of cases.

methods show an optimal behavior for a time separation Δt between two consecutive obser-

vations of about 3 weeks. Finally, we compare the new method with Gauss’s method using synthetic observations without astrometrical error that reproduce the expected scheduling of the Vera Rubin Observatory’s (VRO) Legacy Survey of Space and Time (LSST), characterized by an average Δt of about 4 days. Gauss’s method provides good orbits for a larger number of objects than the topocentric version of Mossotti’s method, which, on the other hand, is faster.

7 Acknowledgments

We thank Dr. Lynne Jones, Dr. Siegfried Eggl, Dr. Sam Cornwall, and Dr. Mario Jurić of the University of Washington (WA) for assistance in identifying, accessing, and understanding the appropriate VRO/LSST simulations. We also thank the anonymous referees for their useful comments. GFG and GB acknowledge the project MIUR-PRIN 20178CJA2B titled “New frontiers of Celestial Mechanics: theory and applications”. GFG, GB and OR have been partially supported by the MSCA-ITN Stardust-R, Grant Agreement n. 813644 under the H2020 research and innovation program.

A Comparison with Mossotti’s original paper

Mossotti	here	Mossotti	here
$(x, y, z)^t$	\mathbf{r}	$(Q''', -Q'', Q')^t$	$\frac{1}{\theta_{12}^2} \left(\frac{u_1}{\theta_{23}}, \frac{u_2}{\theta_{31}}, \frac{u_3}{\theta_{12}} \right)^t$
$(X, Y, Z)^t$	\mathbf{q}	$\begin{pmatrix} B_1''' & B_2''' & B_3''' \\ -B_1'' & -B_2'' & -B_3'' \\ B_1' & B_2' & B_3' \end{pmatrix}$	$\text{adj}(\hat{Q})\hat{P}$
$(\mu, \nu, \omega)^t$	$\hat{\mathbf{q}}$		
R, D	q	$\begin{pmatrix} b_1''' & b_2''' & b_3''' \\ -b_1'' & -b_2'' & -b_3'' \\ b_1' & b_2' & b_3' \end{pmatrix}$	$\text{adj}(\hat{P})\hat{Q}$
$(m, n, o)^t$	$\hat{\rho}$		
δ	ρ		
$\kappa(C''', -C'', C')^t$	\mathbf{c}_\oplus	(ψ', ψ'', ψ''')	$\frac{1}{\kappa} \mathbf{c}^t \hat{P}$
$\kappa(c''', -c'', c')^t$	\mathbf{c}	(χ', χ'', χ''')	$\frac{1}{\kappa} \mathbf{c}_\oplus^t \hat{P}$
$(T''', -T'', T')^t$	\mathbf{T}	$(\varphi', \varphi'', \varphi''')$	$\frac{1}{\kappa} (\mathbf{c}_\oplus - \mathbf{c})^t \hat{Q}$
$(\tau''', -\tau'', \tau')^t$	$\boldsymbol{\tau}$	(Φ', Φ'', Φ''')	$\frac{1}{\kappa} (\mathbf{c}_\oplus - \mathbf{c})^t \hat{P}$
$(\theta''', -\theta'', \theta')^t$	$\boldsymbol{\theta}$		

Table 3: Correspondence table between Mossotti’s and our notation.

References

- [1] A. Celletti and G. Pinzari. Four classical methods for determining planetary elliptic elements: a comparison. *Celestial Mechanics and Dynamical Astronomy*, 93:1–52, 2005.
- [2] A. J. Connolly et al. An end-to-end simulation framework for the Large Synoptic Survey Telescope. In George Z. Angeli and Philippe Dierickx, editors, *Modeling, Systems Engineering, and Project Management for Astronomy VI*, volume 9150 of *Society of Photo-Optical Instrumentation Engineers (SPIE) Conference Series*, page 915014, August 2014.
- [3] F. Delgado and M. A. Reuter. The LSST Scheduler from design to construction. In Alison B. Peck, Robert L. Seaman, and Chris R. Benn, editors, *Observatory Operations: Strategies, Processes, and Systems VI*, volume 9910 of *Society of Photo-Optical Instrumentation Engineers (SPIE) Conference Series*, page 991013, July 2016.
- [4] J. D. Drummond. A test of comet and meteor shower associations. *Icarus*, 45(3):545–553, March 1981.
- [5] C. F. Gauss. *Theoria motus corporum in sectionibus conicis solem ambientium*. Reprinted by Dover publications in 1963, 1809.
- [6] C. F. Gauss. *Werke*, volume VI. Available from Gallica, 1874.
- [7] G. F. Gronchi. Multiple solutions in preliminary orbit determination from three observations. *Celestial Mechanics and Dynamical Astronomy*, 103/4:301–326, 2009.
- [8] G. F. Gronchi, G. Baù, and S. Marò. Orbit determination with the two-body integrals. III. *Celestial Mechanics and Dynamical Astronomy*, 123/2:105–122, 2015.
- [9] G. F. Gronchi, G. Baù, and A. Milani. Keplerian integrals, elimination theory and identification of very short arcs in a large database of optical observations. *Celestial Mechanics and Dynamical Astronomy*, 127/2:211–232, 2017.
- [10] S. Herrick. *Astrodynamics. Vol. 1*. Van Nostrand Reinhold, 1976.
- [11] Ž. Ivezić et al. LSST: From Science Drivers to Reference Design and Anticipated Data Products. *The Astrophysical Journal*, 873(2), 2019.
- [12] J. L. Lagrange. Sur le problème de la détermination des orbites des comètes d’après trois observations. Troisième mémoire. *Nouveaux mémoires de l’Académie royale des sciences et belles-lettres de Berlin*, 1783. Reprinted in *Œuvres de Lagrange*, Gauthier-Villars et fils, Paris (1869), volume 4, pp. 496–532.
- [13] P. S. Laplace. Mémoire sur la détermination des orbites des comètes. *Mémoires de l’Académie royale des sciences de Paris*, 1780. Reprinted in *Œuvres complètes de Laplace*, Gauthier-Villars et fils, Paris (1894), volume 10, pp. 93–146.
- [14] A. Milani and G. F. Gronchi. *Theory of Orbit Determination*. Cambridge Univ. Press, 2010.

- [15] A. Milani, G. F. Gronchi, M. De'michieli Vitturi, and Z. Knežević. Orbit determination with very short arcs. I admissible regions. *Celestial Mechanics and Dynamical Astronomy*, 90(1-2):57–85, September 2004.
- [16] A. Milani, M. E. Sansaturio, G. Tommei, O. Arratia, and S. R. Chesley. Multiple solutions for asteroid orbits: Computational procedure and applications. *Astronomy & Astrophysics*, 431:729–746, February 2005.
- [17] O. F. Mossotti. *Nuova analisi del problema di determinare le orbite dei corpi celesti (1816-1818)*. Domus Galileana, Pisa, 1942. <http://www.mat.uniroma2.it/%7Esimca/Testi/mossotti-nuo-ana.pdf>.
- [18] E. Naghib, P. Yoachim, R. J. Vanderbei, A. J. Connolly, and R. L. Jones. A Framework for Telescope Schedulers: With Applications to the Large Synoptic Survey Telescope. *The Astronomical Journal*, 157(4), 2019.